# Optic Disc Segmentation by Weighting the Vessels Density within the Strongest Candidates

Ali Mohamed Nabil Allam

Information Systems Department
Arab Academy for Science &
Technology (AASTMT)
Cairo, Egypt

Aliaa Abdel-Halim Youssif

Computer Science Department
Helwan University
Cairo, Egypt

Atef Zaki Ghalwash

Computer Science Department
Helwan University
Cairo, Egypt

*Abstract*—**Optic disc segmentation is a key element in automatic screening systems, which facilitates the detection of lesions that affect the interior surface of the eye (i.e. fundus). Therefore, this paper aims to provide a fully automated technique for detecting and segmenting the optic disc. First, the fundus image is preprocessed in order to estimate the approximate location of the optic disc, excluding the positions that doubtfully contain the optic disc. Consequently, the top candidates for the optic disc are detected and then ranked based on their strengths. Afterwards, the vessels density within each candidate is calculated and then weighted according to the candidate's strength, in which the one having the highest score is chosen to be the segmented optic disc. The performance of the proposed segmentation algorithm is evaluated over nine heterogeneous datasets of fundus images, achieving a sensitivity of 94.72%.**

*Keywords—candidates weighting; circularity strength; fundus image; optic disc segmentation; vessels density*

## I. INTRODUCTION

Ophthalmologists are able to diagnose eye diseases using images of the eye fundus which is photographed directly through the eye's pupil via a specialized low-power microscope with an attached camera [1]. Thereby, computer vision systems are developed in order to localize and analyze fundus landmarks, namely the optic nerve head (i.e. optic disc and optic cup), the vasculature (i.e. arteries and veins), and the macular region (i.e. macula and fovea). This segmentation also leads to detecting many eye abnormalities that result in slight-to-major changes of the eye's interior surface, such as exudates, neovascularization, macular edema, notching, etc. fig. 1 illustrates the landmarks of a normal eye fundus:
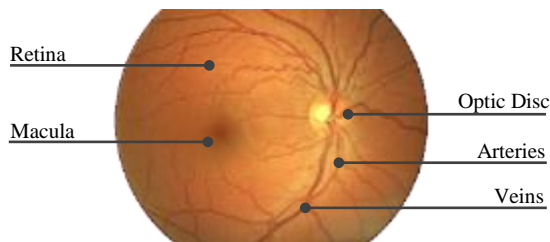


Fig. 1.    Eye fundus image

The optic disc is considered the blind spot of the eye where the optic nerve enters the retina, coming from the brain. As noticed in fig. 1, it is characterized by having a circular shape whose diameter constitutes around one-sixth to one-tenth of the whole fundus width. Also, the optic disc normally appears as a bright region at which the central (i.e. major) retinal vessels originate and radiate above and below. It is typically located towards the left-side or the right-side of a left-eye or a right-eye fundus image, respectively [1], [2].

Furthermore, studying the spatial structure of the optic disc facilitates the diagnosis of some eye diseases. For instance, both the cup-to-disc ratio and the ISNT rim thickness rule (Inferior > Superior > Nasal > Temporal) are two intrapapillary indicators used to diagnose glaucoma which is characterized by the cupping of the optic disc, as well as the thinning of the Inferior and Superior rims (i.e. notching) [1], as noticed in fig. 2-b.
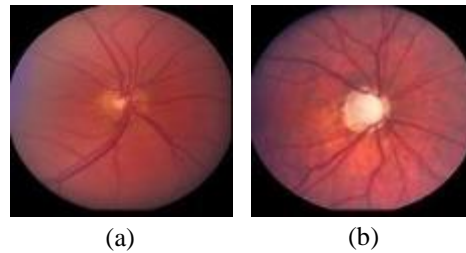


Fig. 2.    (a) Healthy        (b) Glaucoma (cupping & notching)

Also, fig. 3-b shows how diabetic retinopathy can be diagnosed by localizing and inpainting the optic disc, which facilitates the detection of exudates, a key feature of diabetic retinopathy, that are usually confused with the optic disc [2], [3].
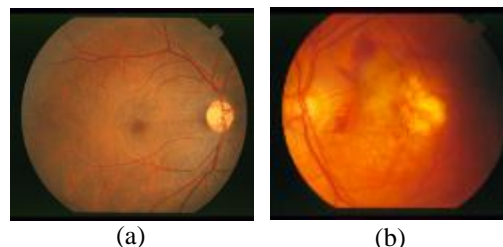


Fig. 3.    (a) Healthy        (b) Diabetic retinopathy (hard exudate)

The remainder of this paper is organized as follows. Section II reviews the previous work pertaining to optic disc segmentation. Section III describes our proposed system for segmenting the optic disc. Finally, the paper presents the

results of the proposed technique, followed by a concluding section.

## II. RELATED WORK

This section reviews the previous work done in optic disc segmentation, since the optic disc is considered the key element in fundus images that leads to detecting and diagnosing serious eye lesions such as glaucoma and diabetic retinopathy, as mentioned in section I. Allam *et al.* [4] presented a survey of optic disc segmentation algorithms through which the main methods reviewed in the literature were categorized as follows:

### A. Techniques based on the properties of optic disc

Such techniques exploit few or all of the main characteristics of the optic disc listed in the previous section, namely its brightness, relative width, roundness, location within the fundus image, or the existence of blood vessels in its vicinity. For instance, Goldbaum *et al.* [5] located the optic disc by observing its bright color as well as detecting the major blood vessels radiating at the top and bottom of it. Walter *et al.* [6] detected the center of the optic disc by identifying the biggest and the brightest region in the fundus image. They detected 47 of the optic discs found in 81 fundus images of the STARE dataset. Exploiting the circularity and the brightness of the optic disc, Zhu *et al.* [7] [1] employed the Circular Hough Transform (CHT) to detect the best-fitting circle for the optic disc which was selected based on an intensity criterion. Their approach succeeded to detect the optic disc in 36 of the 40 images found in the DRIVE dataset, but failed to detect the optic disc in more than half of the images of the STARE dataset. Additionally, Lu [8] localized the boundary and the centroid of the optic disc by observing both the roundness of the optic disc as well as the intensity variation across its boundary. Their approach determined the pixels with the maximum variation along multiple evenly-oriented radial lines of specific length. Their technique was tested over three different datasets, MESSIDOR, STARE, and a subset of ARIA. Also, Yu *et al.* [9] localized the optic disc via a technique of detecting the brightest pixels iteratively, as to be robust against the existence of any bright lesions such as hard exudates. They also set thresholds for the area of the optic disc and its circularity in order to select the optic disc over other nominees. They reported that their approach achieved a detection rate of 95%, although only 40 selected images of the STARE dataset were tested, which means that this rate might have been worse if the whole dataset had been used.

### B. Techniques based on the convergence of blood vessels

Another method for identifying the optic disc is to utilize the spatial relationship between the optic disc and the retinal vessels, since the optic disc is the convergence region of the large blood vessels which branch into more thinner vessels within the fundus image [2]. Accordingly, Hoover *et al.* [10] proposed an approach based on a voting-type technique to detect the optic disc center by identifying the convergence point of the retinal vessels. This algorithm was able to detect the center of the optic disc in 72 of the images of the STARE dataset. Also, ter Haar [11] applied the General Hough Transform (GHT) over the pixels of, as well as the ones near to, the vasculature tree. They examined their technique over the STARE dataset, which detected the optic disc successfully in 58 of the fundus images. The technique presented by Fleming *et al.* [12] approximated the optic disc location by using an elliptic curve of the blood vessels. Then this approximate region of the optic disc was structurally enhanced via the CHT, which successfully identified the optic disc in 98.4% of the fundus images within a locally-based dataset. Rangayyan *et al.* [13], [1] exploited Gabor filtering to extract the retinal vasculature tree, and then they utilized phase portrait modeling to detect the convergence point(s) of the vessels, in which the best-fitting oval for the optic disc was selected using an intensity criterion. Their technique correctly localized the optic disc in all of the 40 images in the DRIVE dataset, and 56 of the 81 images in the STARE dataset.

### C. Techniques based on template matching

Another category of optic disc segmentation methods is based on defining a template image to be matched against a number of candidates in order to select the best-matching image. For instance, Li *et al.* [14] applied the Principal Component Analysis to create an optic disc model called the disc-space. The candidates having the brightest 1% intensity-level were then matched with that disc-space to detect the optic disc. Also, Foracchia *et al.* [15] defined the directionality of the retinal vessels at any certain position via a geometrical model using the coordinates of the optic disc center. The optic disc was successfully located in 79 of the STARE fundus images. In the same direction of exploiting the vessels directionality, Youssif *et al.* [2] presented a technique that matched the directional pattern of the blood vessels in the fundus image. They created a directional map of the retinal vessels which were extracted using a Gaussian matched filter. The optic disc was successfully detected in all the images of the DRIVE dataset, as only one case was missed within the STARE dataset.

Aquino *et al.* [16] employed a voting-type algorithm to locate an initial pixel within the optic disc. Afterwards the algorithm utilized morphological processing and edge detection techniques followed by CHT in order to approximate the circular boundary of the optic disc. This technique successfully detected 86% of the 1200 fundus images in the MESSIDOR dataset. Additionally, Zhang *et al.* [17] obtained a set of candidate vertical regions for the optic disc based on the properties of blood vessels found in the vicinity of the optic disc, namely, the vessels high density, compactness of vertical vascular segments, and the vessels uniform distribution. Afterwards, the vertical coordinate (y-axis) of the optic disc was determined according to the vessels directionality via parabola curve fitting. The optic disc was successfully detected in all images of the DIARETDB0, DIARETDB1 and DRIVE datasets, while only one optic disc was undetected in the STARE dataset.

## III. PROPOSED SYSTEM

The block diagram shown in fig. 4 illustrates our proposed architecture of optic disc segmentation, showing the input data as well as the operations utilized in manipulating the eye fundus images in order to obtain the segmented optic disc. Each of the four block components of this architecture is discussed in detail at the subsequent sections (A, B, C, and D):
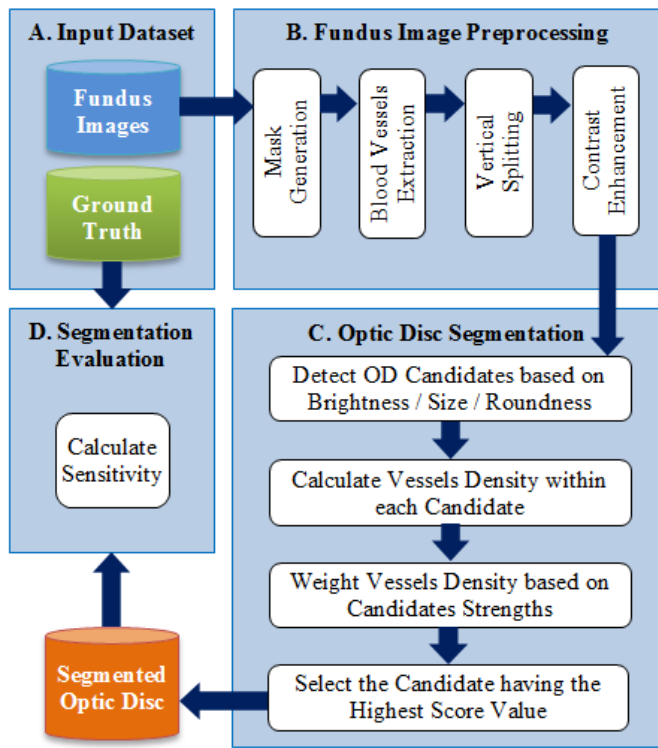
Fig. 4. Block Diagram of Proposed System Architecture

## A. Input Dataset: fundus images and ground truth

The fundus images are the raw data to be processed in order to segment the optic disc. These fundus images are usually accompanied by a ground truth which is used for comparing the results achieved by a computer program against the manual segmentations provided by medical experts. Table I shows a chronological list of the publicly available datasets, which are all used for testing and assessing our proposed segmentation method.

TABLE I. EYE FUNDUS DATASETS

| Dataset Name | No. of Images | FOV | Images Size (in pixels) | Images Format | Ground Truth |
|---|---|---|---|---|---|
| STARE (2000) [18] | 81 | 35° | 700×605 | PPM | OD & BV |
| DRIVE (2004) [19] | 40 | 45° | 565 × 584 | TIFF | BV |
| MESSIDOR (2004) [20] | 1200 | 45° | Set1: 1440×960 Set2: 2240×1488 Set3: 2304×1536 | TIFF | Retinopathy and Macular Edema |
| ONHSD (2004) [21] | 99 | 45° | 760×570 | BMP | OD |
| ARIA (2006) [22], [23] | 143 | 50° | 768×576 | TIFF | OD, BV and Fovea |
| DIARETDB0 & DIARETDB1 (2008) [24] | 215 | 50° | 1500×1152 | PNG | MA, HE and Soft & Hard Exudates |
| DRIONS-DB (2008) [25] | 110 | - | 600×400 | JPG | OD |
| HRF (2009) [26] | 45 | 45° | 3504×2336 | JPG | BV |

FOV = field of view, OD = optic disc, BV = blood vessels, MA = microaneurysms, HE = hemorrhages

## B. Fundus Image Preprocessing

Since the digital fundus images at its raw state cannot be processed directly to localize the optic disc, therefore an image should be prepared first in order to make it ready for further segmentation. For instance, not all datasets are accompanied with the binary mask that defines the region of interest (i.e. semi-oval fundus), neither all datasets include the vasculature tree of the fundus images, which is a vital component in the process of segmenting the optic disc. Accordingly, the following subsections present the main preprocessing steps utilized in the proposed segmentation approach, which intuitively starts with generating the binary masks and extracting the vasculature tree.

### 1) Mask Generation

Binary masks are typically generated and then utilized in order to exclude the black region that surrounds the fundus image from any further useless processing, as shown in fig. 5. The proposed segmentation method exploits the technique presented by ter Haar [11]. First, the red band of the fundus image is thresholded at value of *t=35*. Afterwards, this binary image is processed through the opening, closing and erosion morphological operators using a 3×3 square structuring element.
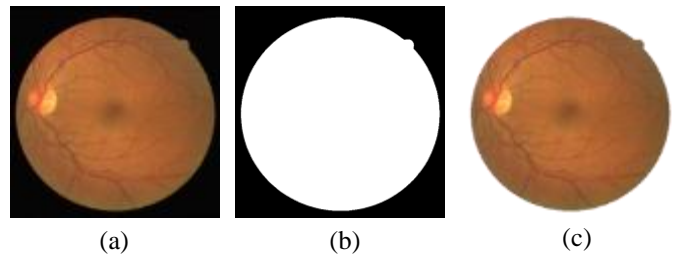


(a)　　　　　(b)　　　　　(c)

Fig. 5. Binary Mask Generation (a) Original imag (b) Binary mask (c) Region of interest

This mask generation approach also succeeds in excluding insignificant artifacts present in some fundus images (e.g. date, time, batch number, etc.). These artifacts were imprinted on the fundus images most likely for labeling and documentation purposes, such as the images of ONHSD and DRIONS-DB.

### 2) Blood Vessels Extraction

The vasculature is roughly extracted via the Canny edge detector using the intensity image specified by the mask, as shown in fig. 6. This step of extracting the vascular tree will be furtherly benefited twice. First, it will be utilized to split the fundus into two vertical halves indicating which half contains the optic disc (part B.3). The second benefit is that these detected retinal vessels will be utilized to calculate the density of vessels within each of the segmented optic disc candidates (part C.2).

### 3) Vertical Splitting

As mentioned previously in section I, the optic disc is typically located towards the left-side or the right-side of a left-eye or a right-eye fundus image, respectively, and from which the major blood vessels originate. Thus, the optic disc is normally located at the half containing more blood vessels than the other (as noticed in fig. 1 and fig. 6).
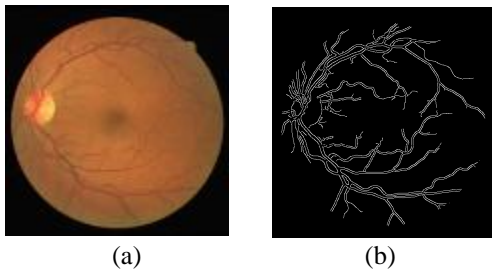
Fig. 6. Vessels Extraction (a) Reference image (b) Extracted blood vessels

Thereby, the fundus image is vertically split into two halves (i.e. left and right), and the half with much blood vessels is selected for further image processing whereas the other one having less vessels is excluded (fig. 7). This splitting approach kills two birds with one stone; first, it greatly reduces all further processing-time to almost 50%. Secondly, it reduces the number of false candidates of the optic disc which may occur in the excluded half. These false candidates may result from artifacts that are similar to the optic disc such as exudates, or may also sometimes occur due to non-uniform illumination (i.e. vignetting effect).
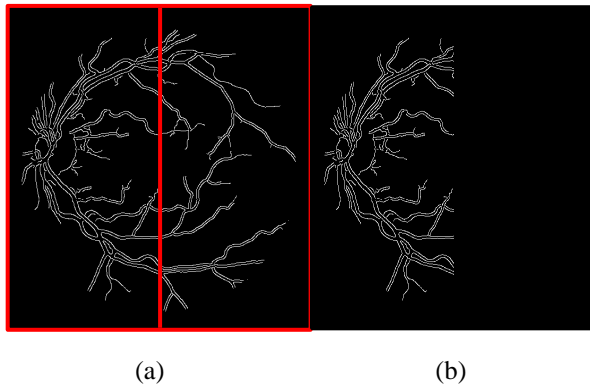


Fig. 7. Vertical Splitting (a) Left and right extracted vessels (b) Selected half

### 4) Contrast Enhancement

In the direction of segmenting the optic disc, the contrast of fundus image is first enhanced in order to improve the segmentation process. At the beginning, the color fundus image is converted to a grayscale intensity image by eliminating the hue and saturation information while retaining the luminance. Consequently, the intensity pixels in this grayscale image are mapped to new values such that 1% of the data is saturated at low and high intensities of the grayscale image. This in turn increases the contrast of the output image, as shown in fig. 8.

### C. Optic Disc Segmentation

This component is the backbone of the system architecture. First, the top three candidates for the optic disc are detected and then ranked based on their circularity strengths. Consequently, the vessels density within each candidate is calculated and then weighted according to the candidate's strength. At the end, the candidate having the highest score is selected as the segmented optic disc.
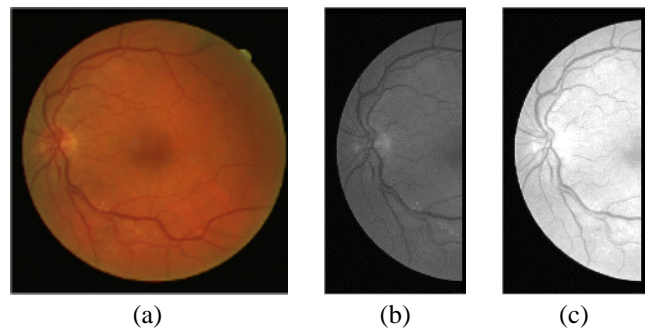


Fig. 8. Contrast Enhancement (a) Original image (b) Intensity image of selected half (c) Adjusted contrast of intensity image

### 1) Detecting Optic Disc Candidates

Identifying the optic disc candidates is the most important step that greatly affects the accuracy of the whole segmentation process. The objective of this process is to detect the top three candidates of the optic disc based on its main spatial properties: its brightness, size, roundness, and before all, its approximate location within the fundus (i.e. left half or right half). Since the approximate location of the optic disc had been already determined previously, therefore this step is only concerned with the other three properties:

- *Brightness:* the contrasted intensity image is converted to a binary image by thresholding it at *t=255*, in order to detect only the bright (white) artifacts in the fundus image.

- *Size:* as mentioned before, the optic disc constitutes one-tenth to one-sixth of the width of the whole fundus image. Accordingly, the algorithm estimates the radius range of the optic disc relative to the width of the fundus image, rounded to the greater integer. For instance, in the DRIVE dataset whose fundus widths are 584 pixels, the radii of the optic discs are estimated within a range of (30 to 50) pixels. The radius range (min-to-max) is estimated as follows:

$$min = ceil\left(\frac{width}{100}\right) \times \frac{10}{2} \qquad (1)$$

$$max = ceil\left(\frac{width}{60}\right) \times \frac{10}{2} \qquad (2)$$

- *Roundness:* because the optic disc is characterized by having a circular shape, the algorithm first applies some morphological opening operators in order to structurally enhance the circular objects in the thresholded image. Consequently, the Circular Hough Transform is utilized in order to detect and localize all the circular shapes specified by the estimated radii.

Based on all these previous spatial properties, the strongest three circular shapes are chosen as the top candidates of the optic disc, and these candidates are then ranked according to their circularity strengths.

### 2) Calculating Vessels Density

It was mentioned before that the major blood vessels radiate from the center of the optic disc. Therefore, the vessels density within each candidate is calculated in order to determine how much blood vessels each candidate contains.

For each of the three optic disc candidates, the corresponding vessels density is calculated as follows:

$$Density = \frac{Size\ (BV)}{Size\ (OD)} \quad\quad (3)$$

where, *Size (BV)* is the number of pixels of the blood vessels inside the detected candidate, and *Size (OD)* is the number of pixels within the candidate optic disc (i.e. the area of the oval).

*3) Weighting Vessels Density*

Having the top three ranked candidates of the optic disc, as well as the vessels density within each candidate, the vessels density is weighted accordingly. First, each candidate is assigned a weight based on its circularity strength. These weights are determined empirically as $w_1 = 1.2$, $w_2 = 1.1$, $w_3 = 1.0$, for the strongest, moderate and weakest candidates, respectively. Consequently, the calculated vessels densities are weighted according to the candidates' strengths, as follows:

$$Score_1 = w_1 \times Density_1 \quad\quad (4)$$
$$Score_2 = w_2 \times Density_2 \qu\quad (5)$$
$$Score_3 = w_3 \times Density_3 \quad\quad (6)$$

*4) Selecting the Segmented Optic Disc*

The final step in the segmentation procedure is to choose one of the candidates to be the optic disc. Each of the figures from fig. 9 to fig. 14, show various examples of selecting the optic disc candidate within healthy and pathological images. (Note: these figures are best viewed within the paper when zoomed to 200% or more). The top three candidates of the optic disc in a fundus image are: the red circle (strongest candidate), the green circle (moderate candidate), and the blue circle (weakest candidate).

Fig. 9 and fig. 10 show examples of how the strongest candidate is selected (red circle). In fig. 9, for instance, the red candidate was promoted and selected as the optic disc due to weighting, although the blue circle has denser blood vessels. Also, fig. 10 shows a good example of how vertical splitting succeeded in excluding the right half which contained a false candidate (i.e. large exudate) that looked like the optic disc.

Fig. 11 and fig. 12 show how the moderate candidate is selected (green circle). These examples emphasize the importance of the vessels density together with the candidates' weights, in order to accurately localize the optic disc in the fundus image. For instance, although the moderate candidate in fig. 11 was not the one with the densest vessels nor the highest weight among other candidates, yet this green candidate was weighted in such a way that it scored a value surpassing those scored by both, the strongest and the weakest candidates.

In the examples shown in fig. 13 and fig. 14, the blue circle was selected although it is the weakest candidate. This is because neither of the two other stronger candidates were weighted highly enough to achieve a score greater than that achieved by the weak (blue) candidate.
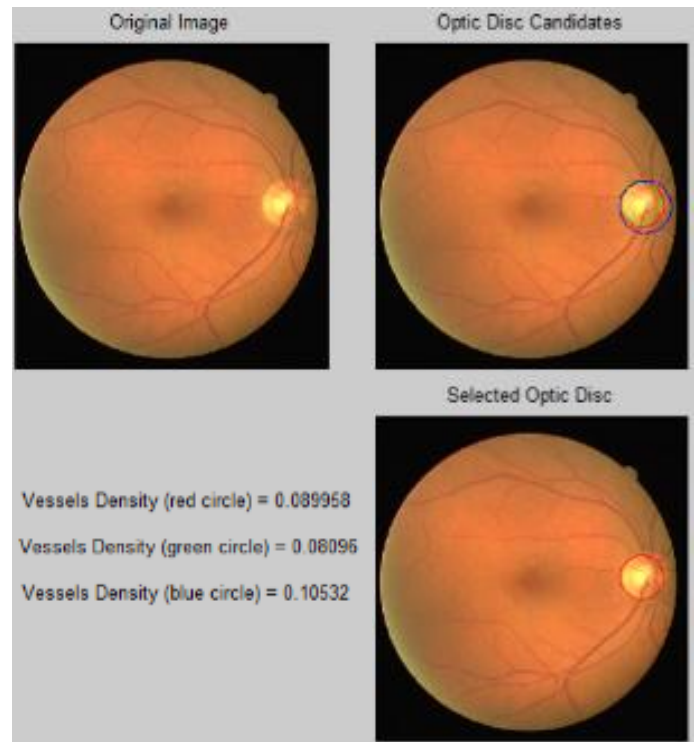


Fig. 9. Example of selecting the strongest candidate in a healthy image (DRIVE: "32_training.tif")
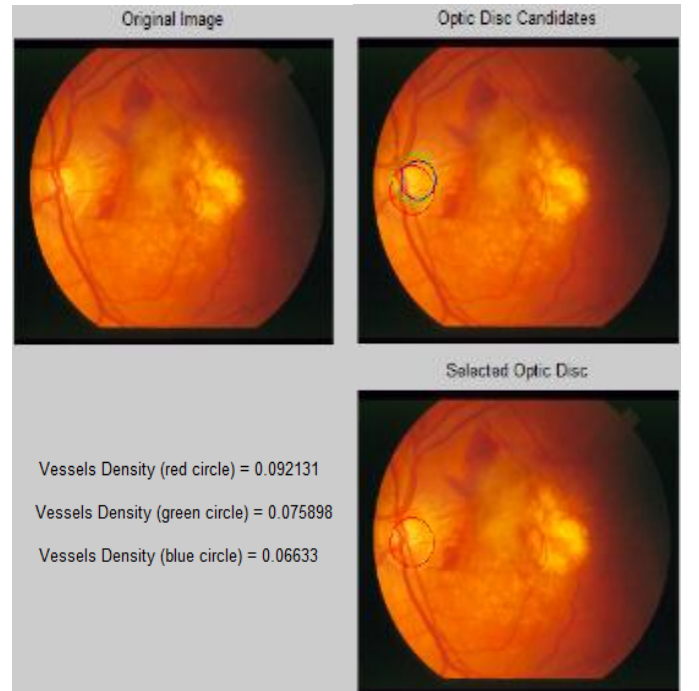


Fig. 10. Example of selecting the strongest candidate in a pathological image (STARE: "im0008.ppm")
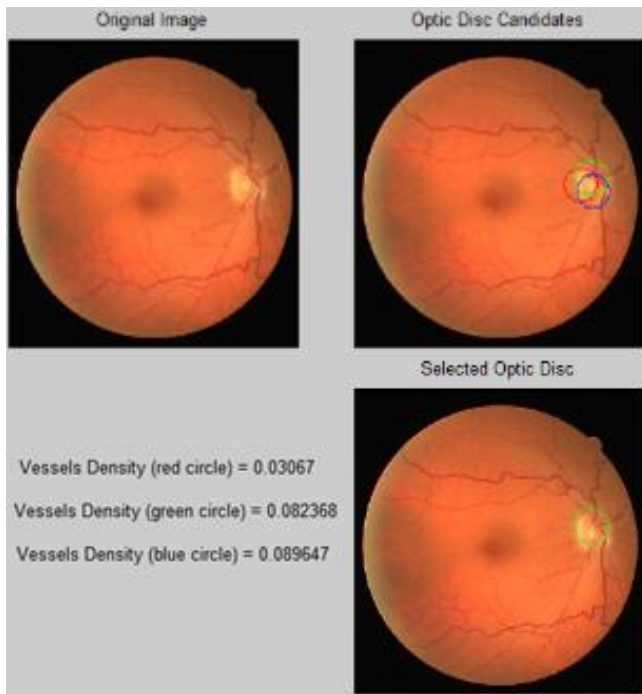
Fig. 11. Example of selecting the moderate candidate in a healthy image (DRIVE: "22_training.tif")
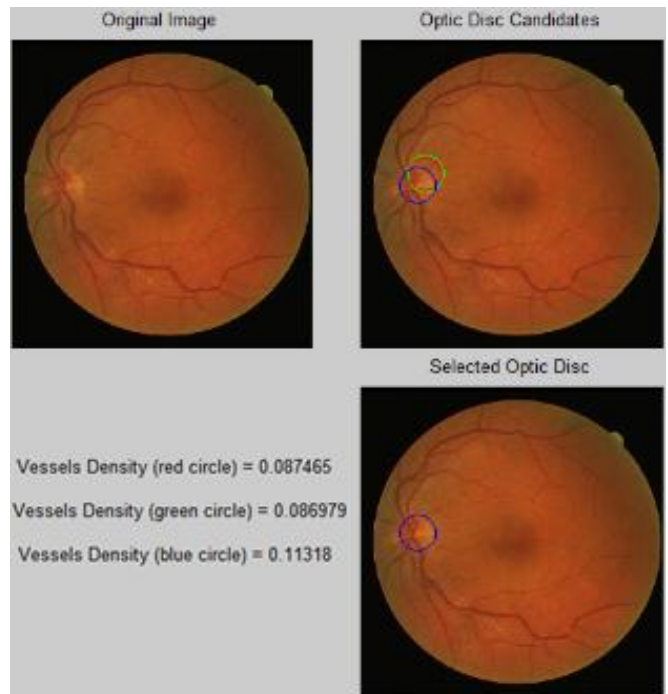


Fig. 13. Example of selecting the weakest candidate in a healthy image (DRIVE: "03_test.tif")
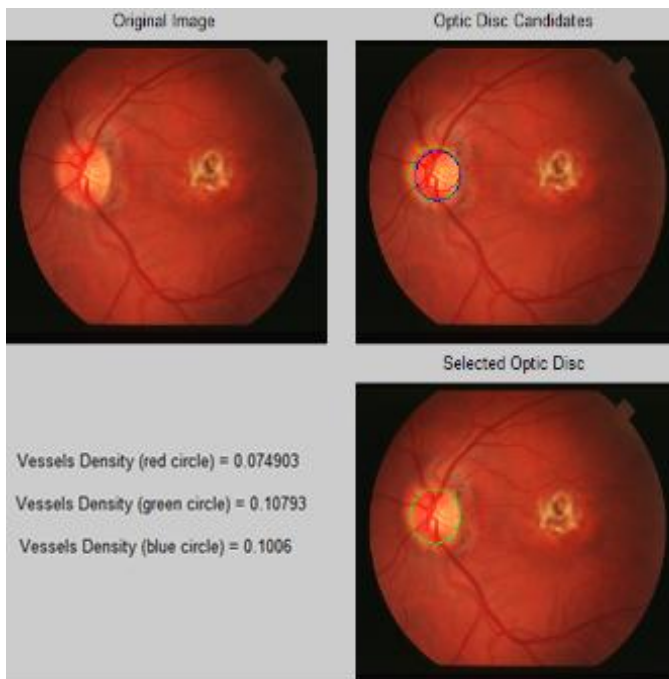


Fig. 12. Example of selecting the moderate candidate in a pathological image (STARE: "im0011.ppm")
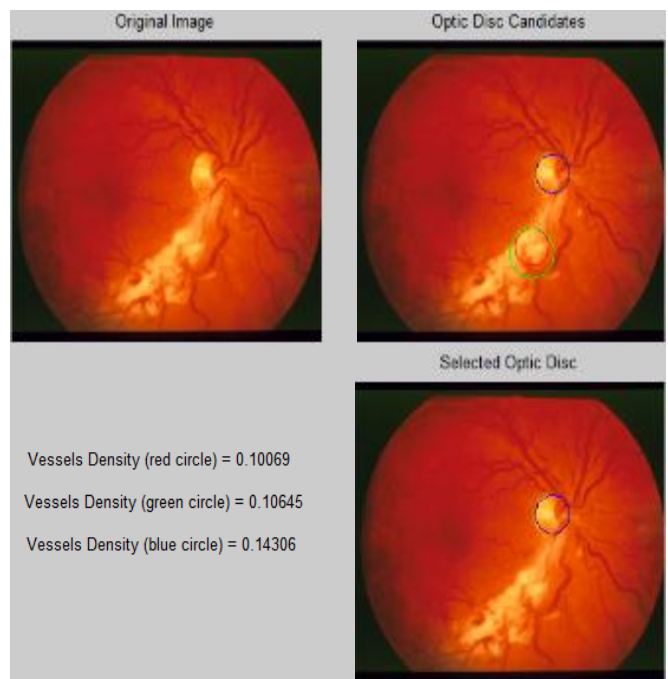


Fig. 14. Example of selecting the weakest candidate in a pathological image (STARE: "im0043.ppm")

*D. Segmentation Evaluation*

In order to evaluate the proposed segmentation algorithm, our produced segmentations are compared against the provided ground truths. The evaluation of the algorithm is measured via "*sensitivity*" which is the true positive rate of detecting the optic disc.

Fig. 15, fig. 16, and fig. 17 show samples from different datasets of fundus images and their corresponding ground truths of the optic disc. It is worth to mention that the ground truth is not always represented in the same manner within all datasets; even some datasets, such as HRF, represent this ground truth textually, rather than showing it graphically.
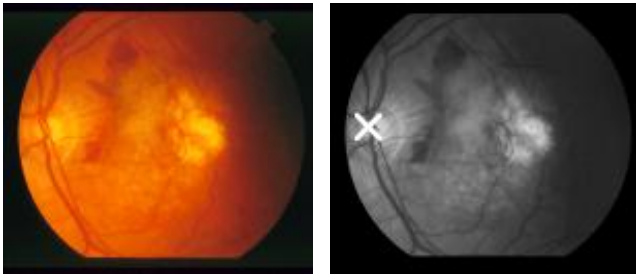
Fig. 15. Example of a fundus image and its corresponding ground truth in STARE dataset
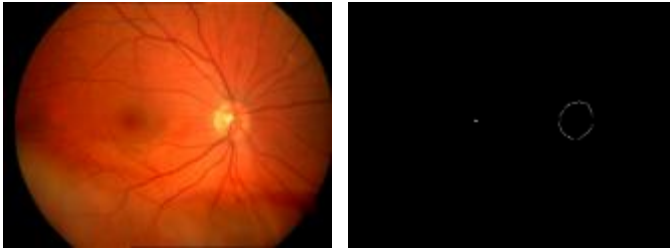


Fig. 16. Example of the fundus image and its corresponding ground truth in ARIA dataset
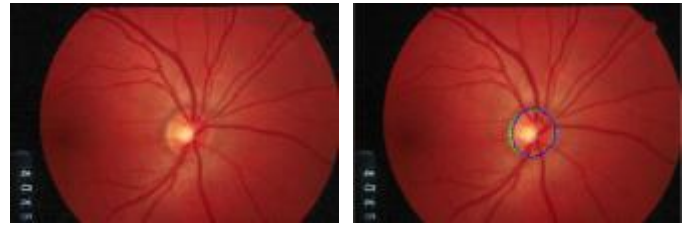


Fig. 17. Example of the fundus image and its corresponding ground truth in DRIONS-DB dataset

## IV. EXPERIMENTAL RESULTS

The proposed algorithm was implemented using MATLAB R2013a under a platform of Windows 10 Pro with a CPU i5-3230M of 2.60 GHz. The system was tested over nine miscellaneous datasets having extremely heterogeneous properties (e.g. image spatial size, image quality, FOV, format, etc.). The purpose of using heterogeneous datasets was to prove the effectiveness of the segmentation algorithm, over any fundus image whatsoever.

Table II distinguishes the results achieved by our proposed approach over the nine different datasets, mainly in terms of the sensitivity and the processing time.

TABLE II. RESULTS OF PROPOSED METHOD

| No. | Dataset Name | No. of Images | No. of Correct Responses | Sensitivity | Processing Time (in seconds) | Avg. Processing Time per Image | No. of Pixels per Image |
|---|---|---|---|---|---|---|---|
| 1 | ARIA | 143 | 121 | 0.8462 | 78.1165 | 0.5463 | 442,368 |
| 2 | DIARETDB0 | 126 | 114 | 0.9048 | 174.4838 | 1.3848 | 1,728,000 |
| 3 | DIARETDB1 | 89 | 79 | 0.8876 | 122.7492 | 1.3792 | 1,728,000 |
| 4 | DRIONS-DB | 110 | 110 | 1.0000 | 40.2961 | 0.3663 | 240,000 |
| 5 | DRIVE | 40 | 39 | 0.9750 | 14.4641 | 0.3616 | 329,960 |
| 6 | HRF | 45 | 42 | 0.9333 | 296.2217 | 6.5827 | 8,185,344 |
| 7a | MESSIDOR (set1) | 400 | 394 | 0.9850 | 933.4118 | 2.3335 | 1,382,400 |
| 7b | MESSIDOR (set2) | 400 | 389 | 0.9725 | 440.6891 | 1.1017 | 3,333,120 |
| 7c | MESSIDOR (set3) | 400 | 390 | 0.9750 | 731.8618 | 1.8297 | 3,538,944 |
| 8 | ONHSD | 99 | 94 | 0.9495 | 56.5776 | 0.5715 | 433,200 |
| 9 | STARE | 81 | 59 | 0.7284 | 45.9078 | 0.5668 | 423,500 |
| | **ALL DATASETS** | **1933** | **1831** | **0.9472** | **2934.7796** | **1.5183** | **-** |

Table III shows a comparison of our proposed method against the different optic disc detection methods reviewed in section II, from the perspective of the detection approach, the employed datasets, and the sensitivity of detecting the optic disc.

TABLE III. RESULTS OF OPTIC DISC DETECTION TECHNIQUES

| No. | Detection Technique | Input Dataset(s) | Sensitivity |
|---|---|---|---|
| 1 | Goldbaum *et al.*, (1996) [5] | None | - |
| 2 | Walter *et al.*, (2001) [6] | Local dataset (30 images) <br> STARE[1] | 0.9000 <br> 0.5802 |
| 3 | Hoover *et al.*, (2003) [10] | STARE | 0.8888 |
| 4 | Foracchia *et al.*, (2004) [15] | STARE | 0.9753 |
| 5 | Li *et al.*, (2004) [14] | Local dataset (89 images) | 0.9888 |
| 6 | Ter Haar, (2005) [11] | Local dataset (191 images) <br> STARE | 0.9634 <br> 0.7160 |
| 7 | Fleming *et al.*, (2007) [12] | Local dataset (1056 images) | 0.9840 |
| 8 | Youssif *et al.*, (2008) [2] | DRIVE <br> STARE | 1.0000 <br> 0.9877 |
| 9 | Aquino *et al.*, (2010) [16] | MESSIDOR | 0.8600 |
| 10 | Rangayyan *et al.*, (2010) [13] | DRIVE <br> STARE | 1.0000 <br> 0.6913 |
| 11 | Zhu *et al.*, (2010) [7] | DRIVE <br> STARE | 0.9000 <br> 0.4444 |

[1] Additional results were obtained from ter Haar [11].

| No. | Detection Technique | Input Dataset(s) | Sensitivity |
|---|---|---|---|
| 12 | Lu, (2011) [8] | ARIA subset (120 images) | 0.9750 |
| | | MESSIDOR | 0.9975 |
| | | STARE | 0.9876 |
| 13 | Yu *et al.*, (2014) [9] | STARE subset (40 images) | 0.9500 |
| 14 | Zhang *et al.*, (2014) [17] | DIARETDB0 | 1.0000 |
| | | DIARETDB1 | 1.0000 |
| | | DRIVE | 1.0000 |
| | | STARE | 0.9877 |
| 15 | *Proposed Method, (2016): Weighting vessels density within the strongest optic disc candidates* | ARIA | 0.8462 |
| | | DIARETDB0 | 0.9048 |
| | | DIARETDB1 | 0.8876 |
| | | DRIONS-DB | 1.0000 |
| | | DRIVE | 0.9750 |
| | | HRF | 0.9333 |
| | | MESSIDOR (3 sets) | 0.9775 |
| | | ONHSD | 0.9495 |
| | | STARE | 0.7284 |

## V. CONCLUSION

The segmentation methods that are solely dependent on the spatial properties of the optic disc (e.g. its circularity, brightness, relative width and location within the fundus image) achieve high detection rates within healthy fundus images that contain no abnormalities. But, these property-based methods are usually unable to detect and localize the optic disc in the presence of bright oval-shaped lesions, such as the exudates, which are confused with the optic disc due to their like-looking structure.

Alternatively, other segmentation techniques, which rely on the convergence of blood vessels or template matching, achieve higher sensitivity rates. This is because the numbers of wrong responses are greatly reduced in the presence of other objects that look like the optic disc.

However, such approaches obviously take more processing time and normally require pre-customized templates or image-dependent parameters.

Thereby, our segmentation approach proposed in this paper benefited the advantages of these different alternatives, in a simple and straightforward way.

It relied on the spatial characteristics of the optic disc, and at the same time, it reduced the number of false candidates in order improve the sensitivity rates within pathological images, and above all, in a fully-automated manner.

The proposed algorithm was tested and evaluated over nine public datasets containing a total of 1933 images. The segmentation algorithm proved its effectiveness by segmenting the optic disc correctly in 1831 images achieving a total sensitivity of 94.72% which was comparable to the results achieved by the other approaches. But more importantly, the implementation of the segmentation algorithm was fully automated regardless of the extreme heterogeneity of the tested datasets (e.g. spatial size, FOV, image quality, etc.); as image-dependent parameters are neither adjusted nor are predefined templates used for the sake of customizing the proposed algorithm over certain datasets.

## REFERENCES

[1] X. Zhu, R. M. Rangayyan and A. L. Ells, "Digital Image Processing for Ophthalmology: Detection of the Optic Nerve Head," in Synthesis Lectures Biomed. Eng., Morgan & Claypool Publishers, 2011.

[2] A. A. A. Youssif, A. Z. Ghalwash and A. A. S. A. Ghoneim, "Optic Disc Detection From Normalized Digital Fundus Images by Means of a Vessels' Direction Matched Filter," IEEE Trans. Med. Imag., vol. 27, no. 1, pp. 11-18, 2008.

[3] G. Schaefer and A. Clos, "Image Analysis for Exudate Detection in Retinal Images," in Biocomputation and Biomedical Informatics: Case Studies and Applications, Medical Information Science Reference, 2010, pp. 198-203.

[4] A. M. N. Allam, A. A. Youssif and A. Z. Ghalwash, "Automatic Segmentation of Optic Disc in Eye Fundus Images: A Survey," Electron. Lett. Comput. Vision Image Anal., vol. 14, no. 1, pp. 1-20, 2015.

[5] M. Goldbaum, S. Moezzi, A. Taylor, S. Chatterjee, J. Boyd, E. Hunter and R. Jain, "Automated diagnosis and image understanding with object extraction, object classification, and inferencing in retinal images," in Proc. IEEE Int. Congr. Image Process., 1996.

[6] T. Walter and J. Klein, "Segmentation of Color Fundus Images of the Human Retina: Detection of the Optic Disc and the Vascular Tree Using Morphological Techniques," in Proc. 2nd Int. Symp. Medical Data Analysis (ISMDA '01), 2001.

[7] X. Zhu, R. M. Rangayyan and A. L. Ells, "Detection of the Optic Nerve Head in Fundus Images of the Retina Using the Hough Transform for Circles," J. Digital Imaging, vol. 23, no. 3, pp. 332-341, June 2010.

[8] S. Lu, "Accurate and Efficient Optic Disc Detection and Segmentation by a Circular Transformation," IEEE Trans. Med. Imag., vol. 30, no. 12, pp. 2126-2133, December 2011.

[9] C.-Y. Yu and S.-S. Yu, "Automatic Localization of the Optic Disc Based on Iterative Brightest Pixels Extraction," in 2014 Int. Symp. Comput. Consumer Control, 2014.

[10] A. Hoover and M. Goldbaum, "Locating the Optic Nerve in a Retinal Image Using the Fuzzy Convergence of the Blood Vessels," IEEE Trans. Med. Imag., vol. 22, no. 8, pp. 951-958, 2003.

[11] F. ter Haar, "Automatic localization of the optic disc in digital colour images of the human retina," 2005.

[12] A. D. Fleming, K. A. Goatman, S. Philip, J. A. Olson and P. F. Sharp, "Automatic detection of retinal anatomy to assist diabetic retinopathy screening," Physics in Medicine and Biology, vol. 52, no. 2, pp. 331-345, January 2007.

[13] R. M. Rangayyan, X. Zhu, F. J. Ayres and A. L. Ells, "Detection of the Optic Nerve Head in Fundus Images of the Retina with Gabor Filters and Phase Portrait Analysis," J. Digital Imaging, vol. 23, no. 4, pp. 438-453, August 2010.

[14] H. Li and O. Chutatape, "Automated Feature Extraction in Color Retinal Images by a Model Based Approach," IEEE Trans. Biomed. Eng., vol. 51, no. 2, pp. 246-254, February 2004.

[15] M. Foracchia, E. Grisan and A. Ruggeri, "Detection of Optic Disc in Retinal Images by Means of a Geometrical Model of Vessel Structure," IEEE Trans. Med. Imag., vol. 23, no. 10, pp. 1189-1195, October 2004.

[16] A. Aquino, M. E. Gegúndez-Arias and D. Marín, "Detecting the Optic Disc Boundary in Digital Fundus Images Using Morphological, Edge Detection, and Feature Extraction Techniques," IEEE Trans. Med. Imag., vol. 29, no. 11, pp. 1860-1869, November 2010.

[17] D. Zhang and Y. Zhao, "Novel Accurate and Fast Optic Disc Detection in Retinal Images with Vessel Distribution and Directional Characteristics," IEEE J. Biomed. Health Informatics, no. 99, 28 October 2014.

[18] M. Goldbaum, "The STARE Project," 2000. [Online]. Available: http://www.parl.clemson.edu/~ahoover/stare/index.html. [Accessed 28 July 2013].

[19] J. J. Staal, M. D. Abramoff, M. Niemeijer, M. A. Viergever and B. van Ginneken, "Ridge Based Vessel Segmentation in Color Images of the Retina," IEEE Trans. Med. Imag., vol. 23, pp. 501-509, 2004.

[20] E. Decencière, X. Zhang, G. Cazuguel, B. Lay, B. Cochener, C. Trone, P. Gain, J. Ordonez-Varela, P. Massin, A. Erginay, B. Charton and J. Klein, "Feedback on a Publicly Distributed Database: The Messidor Database," Image Analysis & Stereology, vol. 33, no. 3, pp. 231-234, 2014.

[21] J. Lowell, A. Hunter, D. Steel, A. Basu, R. Ryder, E. Fletcher and L. Kennedy, "Optic Nerve Head Segmentation," IEEE Tans. Med. Imag., vol. 23, no. 2, pp. 256-264, February 2004.

[22] Y. Zheng, M. H. A. Hijazi and F. Coenen, "Automated ''Disease/No Disease'' Grading of Age-Related Macular Degeneration by an Image Mining Approach," Investigative Ophthalmology & Visual Science, vol. 53, no. 13, pp. 8310-8318, November 2008.

[23] D. J. J. Farnell, F. N. Hatfield, P. Knox, M. Reakes, S. Spencer, D. Parry and S. P. Harding, "Enhancement of blood vessels in digital fundus photographs via the application of multiscale line operators," J. Franklin Inst., vol. 345, no. 7, pp. 748-765, October 2008.

[24] T. Kauppi, V. Kalesnykiene, J. Kamarainen, L. Lensu, I. Sorri, A. Raninen, R. Voutilainen, H. Uusitalo, H. Kalviainen and J. Pietila, "DIARETDB1 diabetic retinopathy database and evaluation protocol".

[25] E. J. Carmona, M. Rincon, J. Garcia-Feijoo and J. M. Martinez-de-la-Casa, "Identification of the optic nerve head with genetic algorithms," Artificial Intell. Medicine, vol. 43, no. 3, pp. 243-259, April 2008.

[26] J. Odstrcilik, R. Kolar, A. Budai, J. Hornegger, J. Jan, J. Gazarek, T. Kubena, P. Cernosek, O. Svoboda and E. Angelopoulou, "Retinal vessel segmentation by improved matched filtering: evaluation on a new high-resolution fundus image database," IET Image Process., vol. 7, no. 4, pp. 373-383, June 2013.